Biochemical Journal (2019) **476** 3069–3080
https://doi.org/10.1042/BCJ20190483

Research Article

The chromogranin A-derived antifungal peptide CGA-N9 induces apoptosis in *Candida tropicalis*

Ruifang Li, Chen Chen, Beibei Zhang, Hongjuan Jing, Zichao Wang, Chunling Wu, Pu Hao, Yong Kuang and Minghang Yang

College of Biological Engineering, Henan University of Technology, Zhengzhou 450001, China

Correspondence: Ruifang Li (lrf@haut.edu.cn)

CGA-N9, a peptide derived from human chromogranin A (CGA), was found to have antimicrobial activity in our previous investigation, but its mechanism of action remains unclear. Herein, the mechanism of action of CGA-N9 was investigated. We found that CGA-N9 induced the depolarization of the cell membrane and uptake of calcium ions into the cytosol and mitochondria. With the disruption of the mitochondrial membrane potential, the generation of intracellular reactive oxygen species (ROS) increased. Accordingly, we assessed apoptotic processes in *Candida tropicalis* cells post-treatment with CGA-N9 and found cytochrome *c* leakage, chromatin condensation and DNA degradation. The interaction of CGA-N9 with DNA *in vitro* showed that CGA-N9 did not degrade DNA but bound to DNA via an electrostatic interaction. In conclusion, CGA-N9 exhibits antifungal activity by inducing apoptosis in *C. tropicalis*.

Introduction

Invasive fungal infections continue to appear as the size of the immunocompromised population increases [1,2]. *Candida tropicalis* is one of only five Candida species accounting for 92% of candidemia cases [3–5]. The number of infections caused by *Candida parapsilosis* and *C. tropicalis* in this population is increasing [3]. Azole drugs are commonly used to treat *Candida* infections [6]. However, the overuse of azole compounds in past decades has promoted the emergence of drug-resistant *Candida* species [7]. Thus, novel anticandidal agents are urgently needed [8,9].

Antimicrobial peptides (AMPs), which are produced by virtually all life forms and are multidimensional defence molecules that are not easily overcome by microorganisms using single-approach resistance strategies, represent almost an inexhaustible source of potential therapeutic agents [10,11]. Chromogranin A (CGA) is a ubiquitous soluble protein in most endocrine cells and neuronal cells. The N-terminus of CGA is reported to have antimicrobial activity [12]. Our previous research demonstrated that CGA-N9, corresponding to the N-terminal amino acid sequence from amino acids 47 to 55 of human CGA, has antimicrobial activity against *Candida* species, *Cryptococcus neoformans* and some gram-positive bacteria [13].

In our previous research, we found that most CGA-N9 passes through the *C. tropicalis* cell membrane via direct cell penetration, whereas the remainder enters through macropinocytosis and sulfate proteoglycan-mediated endocytosis, with a slight contribution from clathrin-mediated endocytosis [13]. The intracellular activity of CGA-N9 after its internalization is still unclear. In the present study, the mechanism of CGA-N9 related to apoptosis in *Candida* was explored.

Received: 28 June 2019
Revised: 4 October 2019
Accepted: 14 October 2019

Accepted Manuscript online: 14 October 2019
Version of Record published: 30 October 2019

PORTLAND PRESS

Biochemical Journal (2019) **476** 3069–3080
https://doi.org/10.1042/BCJ20190483

Materials and methods

Microorganism and materials

C. tropicalis CGMCC2.3739 (Beijing, China) was cultured in Sabouraud dextrose (SD) medium at 28°C for 24 h. CGA-N9 with N-terminal and C-terminal deprotection was synthesized by the solid-phase peptide synthesis method. Peptide purification was performed by high-performance liquid chromatography. Other chemicals used in the present study were of analytical grade and from commercial suppliers.

Depolarization of the cell membrane

The *C. tropicalis* cell membrane depolarization post-CGA-N9 treatment was detected by using DiSC3(5) [14,15]. Briefly, *C. tropicalis* cells in the mid-log phase were suspended in 5 mM HEPES to an OD600 of 0.05. A final concentration of 4 μM DiSC3(5) in DMSO was added when the absorbance was stable. The fluorescence intensity of DiSC3(5) was detected at λex/λem = 600 nm/675 nm at 30 s intervals. CGA-N9 was added to a final concentration of 3.9 μg/ml at the stable and maximal fluorescence intensity. Membrane potential disruption was determined by the change in fluorescence intensity. NaN_3 was used as a positive control, and PBS (20 mM, pH 7.2) was used as a negative control. The measurements were repeated three times.

Detection of calcium ions in the cytosol and mitochondria

Changes in Ca^{2+} levels in the cytosol and mitochondria were detected by the membrane-penetrating Ca^{2+} probes Fluo-4AM and Rhod-2AM (Sigma–Aldrich, Shanghai, China), respectively [16,17]. *C. tropicalis* cells (5×10^6 CFU/ml) in the mid-log phase were incubated with 3.9 μg/ml CGA-N9 for 4 h to 16 h at 28°C in 4 h intervals. H_2O_2 (10 mM) was used as a positive control, and PBS (20 mM, pH 7.2) was used as a negative control. The cells were washed with Krebs buffer (132 mM NaCl, 4 mM KCl, 1.4 mM $MgCl_2$, 6 mM glucose, 10 mM HEPES, 10 mM $NaHCO_3$, 1 mM $CaCl_2$; pH 7.2) containing 0.01% Pluronic F-127 (Sigma–Aldrich, Shanghai, China) and 1% bovine serum albumin. The cells were suspended in Krebs buffer and incubated with 5 μM Fluo-4AM or 10 μM Rhod-2AM at 28°C for 30 min. After washing three times with calcium-free Krebs buffer, the fluorescence of Fluo-4AM (λex/λem = 494 nm/516 nm) and Rhod-2AM (λex/λem = 549 nm/578 nm) was detected using a fluorescence spectrophotometer (Cary Eclipse, Australia). PBS (20 mM, pH 7.2) was used as a negative control, and H_2O_2 was used as a positive control. The measurements were repeated three times.

Assessment of intracellular ROS accumulation

The oxidation-sensitive fluorescent dye dihydrorhodamine-123 (DHR123) was used to detect intracellular ROS accumulation [18]. A total of 5×10^6 CFU/ml *C. tropicalis* cells in the mid-log phase were incubated with 3.9 μg/ml CGA-N9 for 8 h at 28°C. H_2O_2 (10 mM) was used as a positive control, and PBS (20 mM, pH 7.2) was used as a negative control. The cells were stained with 5 μg/ml DHR-123 (Sigma–Aldrich, Shanghai, China) for 1 h at 28°C, avoiding light after washing with 20 mM phosphate-buffered saline (PBS; pH 7.2). The samples were analyzed by a FACSCalibur flow cytometer (BD, U.S.A.) at λex/λem = 507 nm/529 nm.

Mitochondrial membrane potential assay

The Molecular Probes JC-1 dye (Beyotime, Shanghai, China) was used to examine the dissipation of mitochondrial membrane potential in *C. tropicalis* cells [19]. The fluorescence of aggregates and monomers was detected by flow cytometry. Briefly, *C. tropicalis* cells (5×10^6 CFU/ml) in the mid-log phase were incubated with 3.9 μg/ml CGA-N9 at 28°C for 8 h. After washing with 20 mM PBS (pH 7.2), JC-1 at a final concentration of 1× was added to the cell suspension and incubated at 28°C for 20 min. *C. tropicalis* cells treated with 10 mM H_2O_2 were used as a positive control, and those treated with PBS (20 mM, pH 7.2) were used as a negative control. The fluorescence intensity at 525 nm (FL1) or 595 nm (FL2) was recorded with a FACSCalibur flow cytometer (BD, U.S.A.). The ratio of JC-1 aggregate to monomer intensity was calculated, and the data represent the mean ± standard deviation of three independent experiments. Statistical significance was determined by Student's *t*-test. P values <0.05 and <0.01 indicate statistical significance.

Detection of cytochrome *c* release

The mitochondrial and cytosolic Cyt *c* content was isolated via differential velocity centrifugation [20]. Briefly, *C. tropicalis* cells (5×10^6 CFU/ml in the mid-log phase) were incubated with 3.9 μg/ml CGA-N9 for 0, 4, 8, 12

and 16 h at 28°C. The incubated cells were homogeneously dispersed in medium (50 mM Tris, 2 mM ethylenediaminetetraacetic acid, 1 mM phenylmethanesulfonylfluoride; pH 7.5) and then glucose was added to a final concentration of 2%. The suspension was centrifuged for 10 min at 20 000×***g***, and the supernatant and cell pellet were collected. The supernatant was centrifuged at 30 000×***g*** for 45 min to collect the resulting supernatant from the superspeed centrifugation to quantify cytosolic Cyt *c*. The cell pellets obtained from the above step were homogenized in Tris-EDTA buffer (50 mM Tris, 2 mM EDTA; pH 5.0) and centrifuged at 7727×***g*** for 30 s. The resulting pellet was suspended in 2 mg/ml Tris-EDTA buffer to quantify mitochondrial Cyt *c*. Ascorbic acid was added to a final concentration of 500 mg/ml for 5 min to reduce the Cyt *c* in the cytosolic and mitochondrial samples. The absorbance at 550 nm was measured with a spectrophotometer (UV1800; AOXI, Shanghai, China) to determine the relative quantities of reduced cytoplasmic and mitochondrial Cyt *c* in the samples. The Cyt *c* content changes in the mitochondria and cytosol mediated by CGA-N9 were analyzed to estimate Cyt *c* release from mitochondria to the cytosol.

Detection of nuclear condensation

Nuclear condensation was assessed by using 4,6-diamidino-2-phenylindole (DAPI) staining (Sigma–Aldrich, Shanghai, China) [21]. *C. tropicalis* cells (5×10^6 CFU/ml) in the mid-log phase were incubated with 3.9 μg/ml CGA-N9 for 4, 8, 12 and 16 h at 28°C. *C. tropicalis* cells that had not undergone CGA-N9 treatment were used as a control. After washing with PBS (10 mM, pH 7.2), the cells were stained with 50 μg/ml DAPI for 20 min in the dark. The samples were then observed using a laser scanning confocal microscope (Olympus FA100, U.S.A) at λex/λem = 358 nm/461 nm.

TUNEL assay

The terminal dexynucleotidyl transferase (TdT)-mediated dUTP nick-end labelling (TUNEL) assay was employed to detect chromosome fragmentation [22]. A total of 5×10^6 CFU/ml *C. tropicalis* cells in log phase were incubated with 3.9 μg/ml CGA-N9 at 28°C for 4, 8, 12 and 16 h. After washing with PBS (10 mM, pH 7.2), the cell pellets were fixed with 3.6% paraformaldehyde for 30 min. After incubation with 0.3% Triton X-100, the cell pellets were treated with 50 μl TUNEL reaction mixture for 2.5 h at 37°C in darkness. After washing, the samples were observed using a laser scanning confocal microscope (Olympus FA100, U.S.A.) at λex/λem = 495 nm/519 nm. *C. tropicalis* cells treated with PBS (10 mM, pH 7.2) for 16 h were used as a negative control, and cells treated with 2.5 mM H_2O_2 for 16 h were used as a positive control.

The fluorescence intensity was assessed by fluorescence spectrophotometry (λex/λem = 495 nm/519 nm) to quantitate DNA labelling.

Gel retardation test

A gel retardation test was used to assess the effect of CGA-N9 on DNA structure and binding [23]. Briefly, 100 ng/μl chromosomal DNA isolated from *C. tropicalis* cells was incubated with CGA-N9 at 1 × minimum inhibitory concentration (MIC), 2 × MIC, 4 × MIC, 8 × MIC, 16 × MIC, and 32 × MIC at room temperature for 12 h. The samples were subjected to gel electrophoresis at 50 V for 30 min. The gel was stained with EB. The migration of DNA was observed under ultraviolet light at a wavelength of 302 nm.

Ultraviolet spectrum assay

CGA-N9 at 3.9 μg/ml was incubated with *C. tropicalis* chromosomal DNA (0 ng/μl, 1.25 ng/μl, 2.5 ng/μl, 5 ng/μl, 10 ng/μl, and 20 ng/μl) for 1 h. The absorbance of the mixture was recorded by an ultraviolet spectrophotometer at wavelengths of 190–350 nm [24].

Statistic analysis

Data are presented as the mean ± standard deviation from three independent experiments. Statistical significance was determined by Student's *t*-test. P values <0.05 and <0.01 indicate statistical significance.

Results

Cell membrane depolarization

The membrane potential-sensitive fluorescent probe 3,3′-dipropylthiadicarbocyanine iodide (DiSC3(5)) concentrates in the cytoplasmic membrane in a membrane potential-dependent manner, which results in the self-quenching of

Biochemical Journal (2019) **476** 3069–3080
https://doi.org/10.1042/BCJ20190483

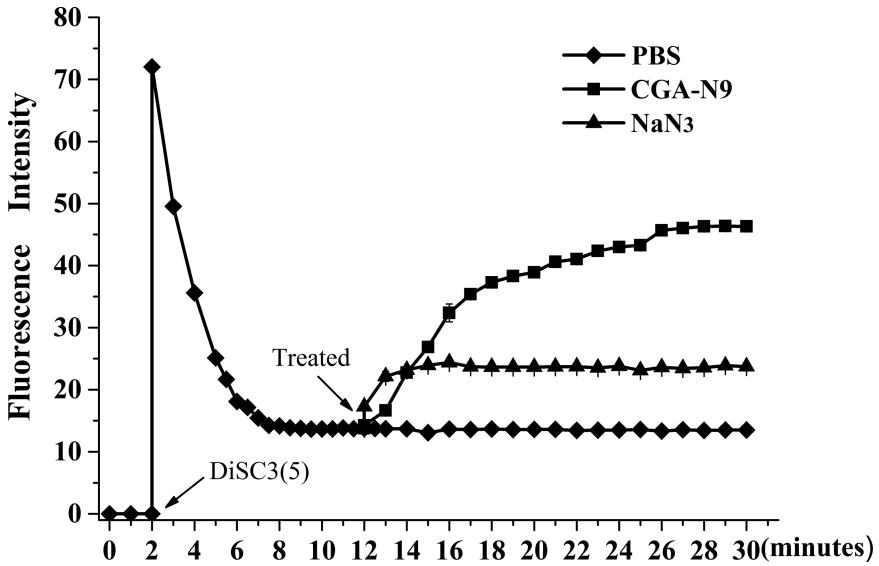

Figure 1. Membrane depolarization of *C. tropicalis* post-CGA-N9 treatment.

The fluorescence of the membrane potential-sensitive dye DiSC3–5 was measured to assess the cell membrane depolarization. A final concentration of 4 μM DiSC3(5) was added to the *C. tropicalis* cell suspension when the absorbance was stable. The fluorescence intensity of DiSC3(5) was detected at λex/λem = 600 nm/675 nm at 30 s intervals. CGA-N9 was added to a final concentration of 3.9 μg/ml at the stable and maximal fluorescence intensity. Membrane potential disruption was determined by the change in fluorescence intensity. NaN_3 was used as a positive control, and PBS (20 mM, pH 7.2) was used as a negative control.

the fluorescence. Once the membrane is depolarized, the dye dissociates into the buffer solution, which causes an increase in fluorescence intensity [15]. As shown in Figure 1, there was a sharp increase in the fluorescence intensity after the addition of DiSC3(5). The fluorescence intensity quickly decreased at the end of the DiSC3(5) addition period because of the self-quenching of the fluorescence. There was a balance of DiSC3(5) monomers and polymers. The fluorescence intensity tended to be stable until CGA-N9 depolarized the cell membrane and disturbed the balance of DiSC3(5) monomers and aggregates. The dye dissociated into the buffer, which caused an increase in the fluorescence intensity.

Disruption of calcium homeostasis

Cell membrane depolarization increases the cellular uptake of calcium, which disrupts cellular calcium homeostasis [25]. The Ca^{2+}-sensitive fluorescent dyes Fluo-4AM (cytoplasmic) and Rhod-2AM (mitochondrial) were used to measure cytosolic and mitochondrial Ca^{2+} levels, respectively. Compared with those of the control cells, cytosolic and mitochondrial Ca^{2+} levels increased in a time-dependent manner in CGA-N9-treated cells and notably increased at 8 h post-treatment with CGA-N9 (Figure 2), indicating that CGA-N9 induces an influx of Ca^{2+} into cells to disrupt mitochondrial and cytosolic Ca^{2+} homeostasis [26].

CGA-N9 induces ROS accumulation

Calcium homeostasis dysregulation causes excess ROS accumulation in cells, which induces mitochondrial dysfunction and apoptosis [27,28]. The ROS level in *C. tropicalis* cells post-treatment with CGA-N9 was evaluated by assessing DHR123 fluorescence intensity, whereby an increase in DHR123 intensity reflects an increase in ROS production. Compared with untreated control cells, CGA-N9-treated cells displayed a sharp increase in ROS accumulation, which peaked at 8 h post-treatment (Figure 3). These results indicate that CGA-N9 treatment-induced ROS accumulation in *C. tropicalis* cells. Therefore, CGA-N9 promotes apoptosis in yeast cells by inducing ROS accumulation.

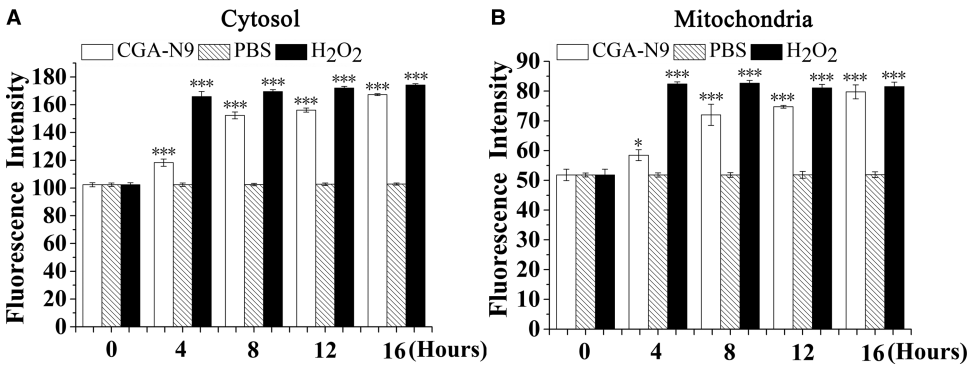

Figure 2. Effect of CGA-N9 on Ca^{2+} levels of *C. tropicalis*.

Approximately 1×10^6 *C. tropicalis* cells were incubated with 3.9 μg/ml CGA-N9 at 28°C for 4, 8, 12 and 16 h. The cytosolic and mitochondrial Ca^{2+} levels were assessed by measuring Fluo-4AM (Ex/Em = 340 nm/510 nm) and Rhod-2AM (Ex/Em = 550 nm/580 nm) intensity, respectively. Relative levels of (A) cytoplasmic calcium ions and (B) mitochondrial calcium ions. PBS (20 mM, pH 7.2) was used as a negative control, and H_2O_2 was used as a positive control. Data represent the mean ± standard deviation of three independent experiments. * $P < 0.05$, *** $P < 0.001$ (Student's *t*-test).

Mitochondrial membrane potential disruption

The dysregulation of mitochondrial Ca^{2+} homeostasis is now recognized as a key effect of ROS accumulation and increased mitochondrial membrane permeability in several pathologies [25,29]. The lipophilic cationic dye JC-1 exists as aggregates (red fluorescence, 595 nm) in cells with polarized mitochondria but as monomers

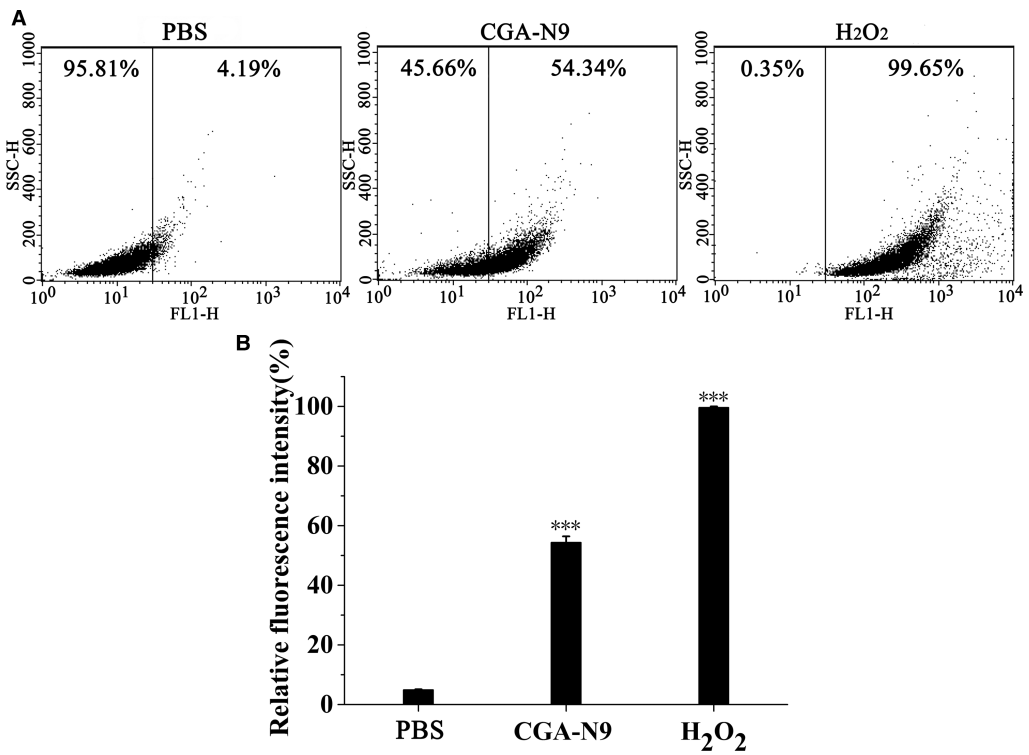

Figure 3. ROS accumulation in *C. tropicalis* cells 8 h post-treatment with CGA-N9.

(**A**) Approximately 1×10^6 CFU/ml *C. tropicalis* cells were incubated with 3.9 μg/ml CGA-N9 or 10 mM H_2O_2 for 8 h at 28°C. Intracellular ROS levels were detected by flow cytometry using dihydrorhodamine-123. Increases in fluorescence intensity indicate increases in ROS levels. (**B**) Data represent the mean ± standard deviation of three independent experiments. *** $P < 0.001$ (Student's *t*-test).

Biochemical Journal (2019) **476** 3069–3080
https://doi.org/10.1042/BCJ20190483

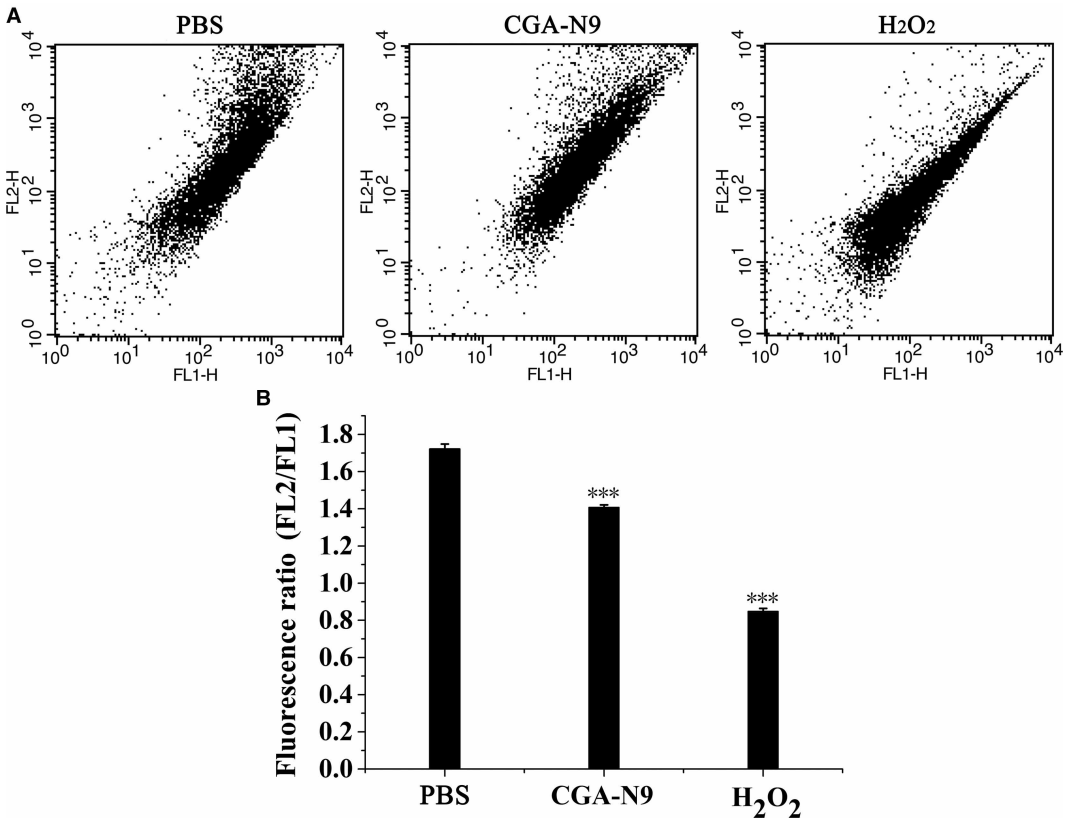

Figure 4. Mitochondrial membrane potential disruption in *C. tropicalis* post-treatment with CGA-N9.

(**A**) Approximately 1×10^6 *C. tropicalis* cells were incubated with 3.9 μg/ml CGA-N9 or 10 mM H_2O_2 for 10 h at 28°C; mitochondrial membrane potential levels were detected by flow cytometry using JC-1. A decrease in the ratio of FL2 to FL1 was interpreted as mitochondrial depolarization. (**B**) Data represent the mean ± standard deviation of three independent experiments. *** $P < 0.001$ (Student's *t*-test).

(green fluorescence, 525 nm) in apoptotic cells with mitochondrial membrane potential disruption [30]. A decrease in the ratio of aggregates to monomers reflects the level of mitochondrial membrane potential disruption. In this study, the fluorescence of JC-1 aggregates (FL2) and monomers (FL1) was detected by flow cytometry. The fluorescence ratios of FL2/FL1 in cells treated with CGA-N9 and H_2O_2 for 8 h were 1.41 and 0.85, respectively, which is lower than that (1.72) of the control cells (Figure 4). These results indicate that CGA-N9 induces mitochondrial membrane potential disruption.

Cytochrome *c* release from mitochondria into the cytosol

The release of Cyt *c* from mitochondria into the cytosol is an important feature of mitochondrial dysfunction, which is followed by apoptosis [17,31]. The changes in the levels of cytosolic and mitochondrial Cyt *c* were quantified according to the recorded ultraviolet absorbance. As shown in Figure 5, the relative quantity of Cyt *c* in the cytoplasm increased, while the relative quantity of Cyt *c* in mitochondria decreased in response to CGA-N9 treatment. At 12 h after treatment of *C. tropicalis* cells with CGA-N9, Cyt *c* leakage into the cytoplasm from mitochondria reached the maximal level.

Chromatin condensation

C. tropicalis cells were stained with the membrane-penetrating dye DAPI, which binds to DNA [32]. The results are shown in Figure 6. DAPI-bound chromatin DNA was distributed homogeneously at the early stage of CGA-N9 treatment. Upon incubation with CGA-N9, the DAPI fluorescence condensed in the cells, which

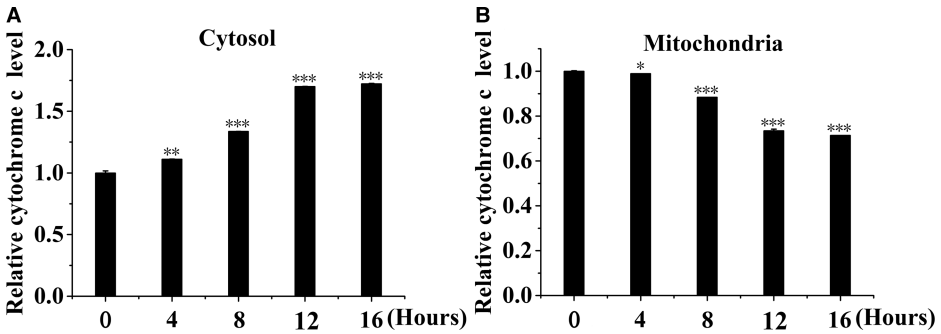

Figure 5. CGA-N9 induces Cyt c release from mitochondria into the cytoplasm.

C. tropicalis cells were incubated with 3.9 μg/ml CGA-N9 for 0, 4, 8, 10 and 16 h at 28°C. The Cyt *c* levels in mitochondria and the cytoplasm were detected by measuring absorbance at 550 nm. Relative levels of (**A**) cytoplasmic Cyt *c* and (**B**) mitochondrial Cyt *c*. Data represent the mean ± standard deviation of three independent experiments. * $P < 0.05$, ** $P < 0.01$ and *** $P < 0.001$ (Student's *t*-test).

indicates chromatin condensation in *C. tropicalis* cells. This result indicates a late apoptotic stage phenotype in *C. tropicalis* cells after treatment with CGA-N9.

DNA degradation

The degradation of nuclear DNA produces free 3′-OH. Under the catalysis of terminal deoxynucleotidyl transferase, exposed free 3′-OH produced by DNA fragmentation reacts with FITC-labelled dUTP [33]. As shown in Figure 7, increased dUTP-FITC fluorescence in *C. tropicalis* cells was observed after treatment with CGA-N9 in a time-dependent manner. This result demonstrates that chromosomal DNA degraded after treatment with CGA-N9, as the dUTP-FITC conjugate binds to free the 3′-OH of the degraded DNA fragment.

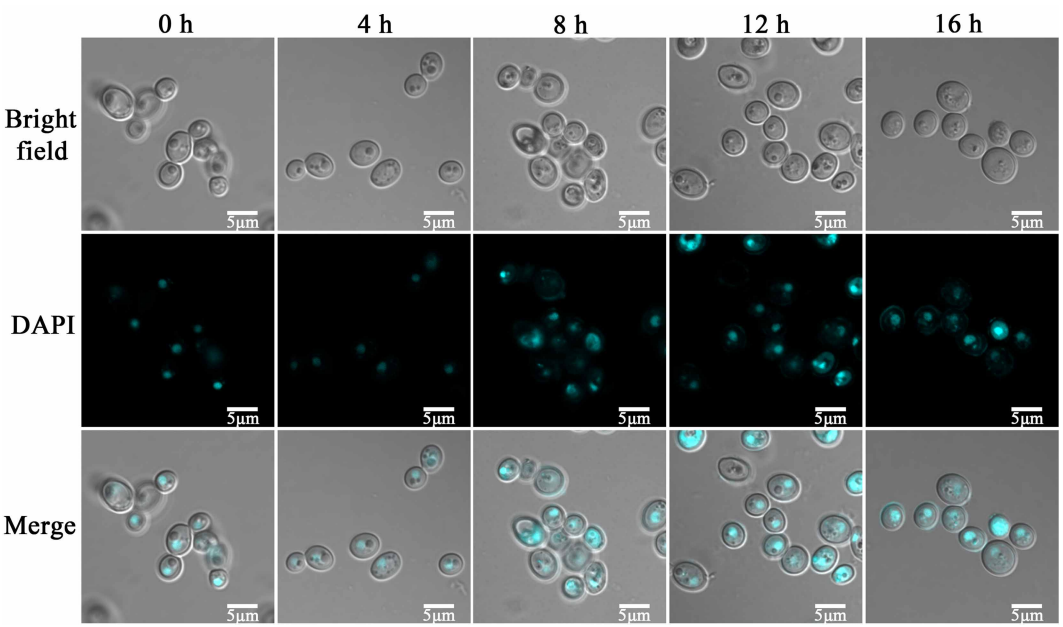

Figure 6. Detection of nuclear DNA condensation in *C. tropicalis* cells treated with CGA-N9.

Approximately 1×10^6 CFU/ml *C. tropicalis* cells in log phase were treated with 3.9 μg/ml CGA-N9, and chromatin condensation was visualized via DAPI staining by laser scanning confocal microscopy. *C. tropicalis* cells not treated with CGA-N12 were used as a control.

Biochemical Journal (2019) **476** 3069–3080
https://doi.org/10.1042/BCJ20190483

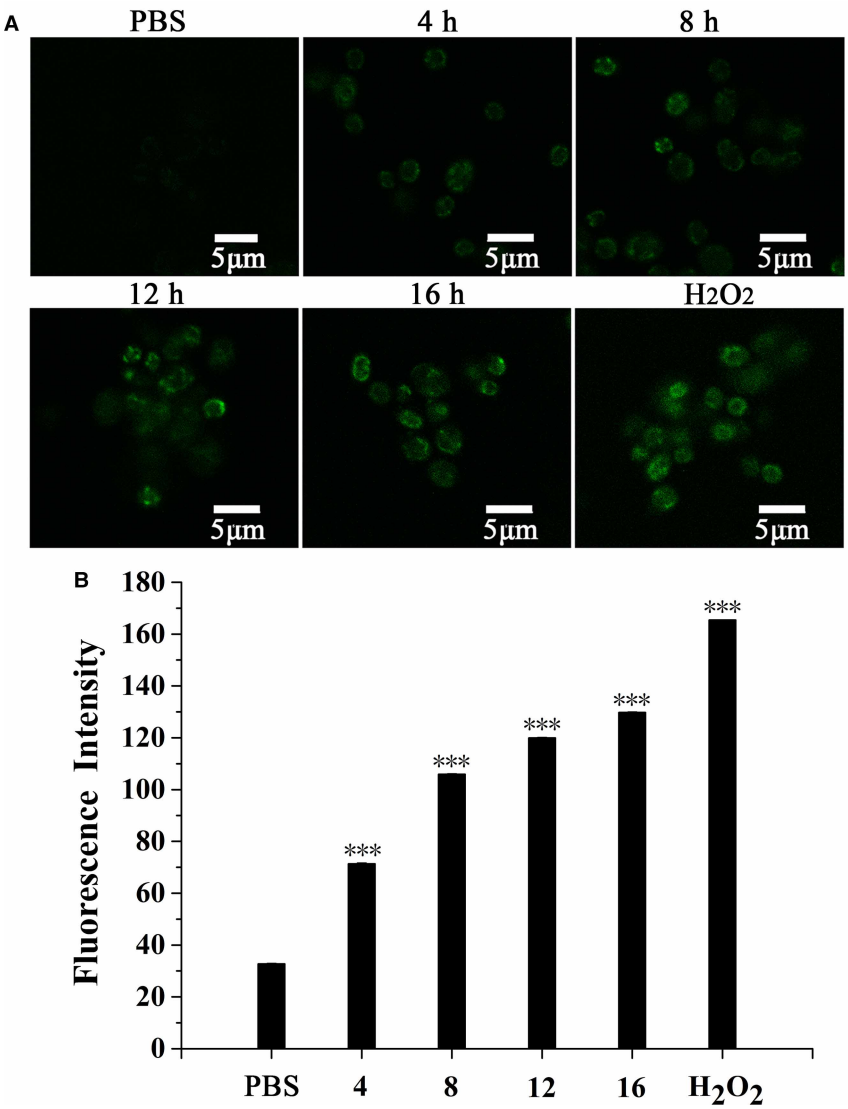

Figure 7. Fluorescence intensity of the damaged DNA assessed by TUNEL staining.

A total of 5×10^6 CFU/ml *C. tropicalis* cells in log phase were incubated with 3.9 μg/ml CGA-N9 at 28°C for 4, 8, 12 and 16 h. Cell pellets were fixed with 3.6% paraformaldehyde then treated with 0.3% Triton X-100. The cell pellets were treated with 50 μl TUNEL reaction mixture for 2.5 h at 37°C in darkness. The cell fluorescence images (**A**) and intensities (**B**) were obtained using a laser scanning confocal microscope (Olympus FA100, U.S.A.) at λex/λem = 495 nm/519 nm. *C. tropicalis* cells treated with PBS (20 mM, pH 7.2) for 16 h were used as a negative control, and cells treated with 2.5 mM H_2O_2 were used as a positive control. Data represent the mean ± standard deviation of three independent experiments. *** $P < 0.001$ (Student's *t*-test).

Interaction of CGA-N9 with DNA

The interaction of CGA-N9 with chromosomal DNA was examined *in vitro*. DNA electrophoretic migration was performed to assess the binding of CGA-N9 to DNA. After incubation with CGA-N9, there was no DNA migration retardation, and DNA ladder bands were observed even up to a CGA-N9 concentration of 8 × MIC. However, no DNA mobility was observed on the gel when the CGA-N9 concentration was greater than 16 × MIC (Figure 8). This result demonstrates that CGA-N9 does not damage the DNA structure and inhibits its separation by gel electrophoresis only at high concentrations. We speculate that CGA-N9 binds only weakly to DNA.

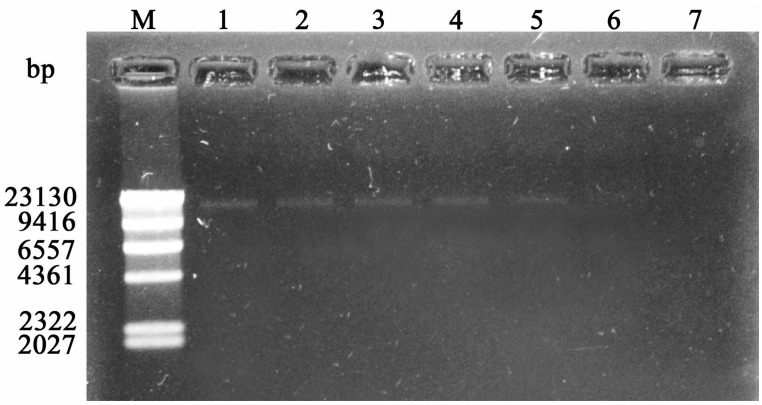

Figure 8. Interaction of DNA with CGA-N9.

A total of 100 μg/ml of isolated chromosomal DNA from *C. tropicalis* was incubated with different concentrations of CGA-N9 for 12 h at room temperature. The mixture was subjected to gel electrophoresis at 50 V for 30 min. The gel was stained with EB and observed under an ultraviolet spectrophotometer at a wavelength of 302 nm. M. λDNA/Hind III; 1. A negative control without CGA-N9; 2. 1 × MIC CGA-N9; 3. 2 × MIC CGA-N9; 4. 4 × MIC CGA-N9; 5. 8 × MIC CGA-N9; 6. 16 × MIC CGA-N9; 7. 32 × MIC CGA-N9.

There will be a redshift of characteristic absorption if a small molecule is embedded in DNA [34]. To investigate the direct interaction between CGA-N9 and DNA, ultraviolet spectrometry was performed to detect the spectral changes of CGA-N9. Compared with the control absorption spectrum, the absorption spectrum of CGA-N9-bound DNA increased, but a redshift was not obvious (Figure 9). Therefore, groove and intercalation binding modes of CGA-N9 with DNA were excluded. Combined with the result of the gel retardation assay, this result suggests that electrostatic interactions formed between positively charged CGA-N9 and negatively charged DNA, and the complex blocked the mobility of the DNA during gel electrophoresis.

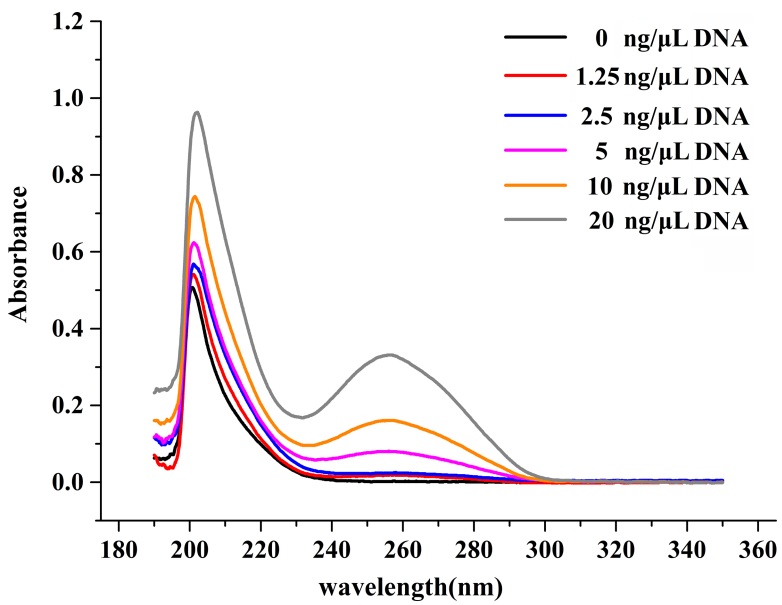

Figure 9. UV absorbance spectra of CGA-N9.

CGA-N9 (3.9 μg/ml) was incubated with different concentrations of *C. tropicalis* chromosomal DNA for 1 h at room temperature. The ultraviolet absorbance of CGA-N9 was recorded using an ultraviolet spectrophotometer at wavelengths of 190 nm–250 nm.

Biochemical Journal (2019) **476** 3069–3080
https://doi.org/10.1042/BCJ20190483

Discussion

Our previous research demonstrated that most CGA-N9 passes through the *C. tropicalis* cell membrane via direct cell penetration [13]. Herein, the interaction of CGA-N9 and cell membrane disturbed the cell membrane permeability.

Apoptosis is a reported mechanism of many AMPs [18,35,36]. Ca^{2+} is a significant regulator of various cellular processes in all eukaryotic cells and a core component of the mitochondrial functional effect [25,29]. Cell membrane depolarization induces Ca^{2+} uptake via the plasma membrane voltage-gated Ca^{2+} channel (Cch1/Mid1 complex) and other unknown transporters [25,37]. The specific Ca^{2+} transport system in the mitochondria membrane aids Ca^{2+} influx into mitochondria. Ca^{2+} homeostasis is often regarded as the initial signal of apoptosis, and oxidative stress is closely related to excessive accumulation of Ca^{2+} in cells [25,29]. Conversely, overloading of Ca^{2+} stimulates oxidative phosphorylation of mitochondria, which increases mitochondrial activity stress; consequently, mitochondrial oxygen consumption increases, resulting in increased ROS production [29,37,38]. CGA-N9 disturbs calcium haemostasis in a time-dependent manner, which corresponds to its bactericidal kinetics [13].

The accumulation of Ca^{2+} induces an increasein intracellular ROS levels. Ca^{2+} and ROS are two key signalling molecules mediating apoptosis, which can cause mitochondrial dysfunction. Ca^{2+}-induced ROS production is an early apoptotic event [33]. In addition to damaging mitochondria, ROS can also cause DNA fragmentation, nuclear damage and dysfunction of macromolecular substances, such as proteins, leading to cell death [19,39]. Because of the lack of a Ca^{2+} unidirectional transporter (MCU) in the yeast mitochondrial membrane [25] for the rapid balance of Ca^{2+} between the cytoplasm and the mitochondrial matrix, Ca^{2+} transfers through the mitochondrial permeability transition pore (mPTP). Increased Ca^{2+} uptake eventually leads to the continuous opening of the mPTP and disturbed mitochondrial Ca^{2+} homeostasis, resulting in mitochondrial extracorporeal membrane swelling and the release of intermembrane proteins, such as Cyt *c*, and other mitochondrial content [25]. In the present study, after treatment with CGA-N9, we detected ROS accumulation and mitochondrial Ca^{2+} homeostasis dysregulation in *C. tropicalis* cells.

Mitochondria are important cellular organelles. Increased cytosolic Ca^{2+} and ROS generation are triggering signals that lead to mitochondrial permeabilization and the release of proapoptotic factors [25,29,40]. The disruption of mitochondrial membrane potential is closely related to the production of ROS in mitochondria [41]. Endogenous oxidative stress directly causes the opening of the mPTPs, followed by the triggering of a series of apoptotic events, such as the leakage of the apoptotic signalling molecule Cyt *c* and certain inducible apoptotic factors into the cytoplasm, which act on the corresponding targets and ultimately induce apoptosis [26,42–44]. In this study, the increased cytosolic Ca^{2+} influx and ROS accumulation after CGA-N9 treatment promoted the disruption of the mitochondrial membrane potential, which is a sign of early apoptosis [45].

Cyt *c* release from the outer surface of mitochondria into the cytoplasm is a key signalling event in the apoptosis pathway [46]. Although certain studies have suggested that Cyt *c* is involved in apoptosis in yeast [16,47], it is not clearly understood whether Cyt *c* participates in yeast apoptosis in the same way that it participates in apoptosis in mammalian cells [47]. No evidence has demonstrated that Cyt *c* can initiate the caspase activation cascade once released into the cytosol by active metacaspase in yeast [25].

Intracellularly accumulated ROS mainly attack the nucleic acids of chromosomes, resulting in single- or double-stranded DNA breaks [28,43,48]. DNA fragmentation and nuclear condensation are typical features of late apoptosis [41,49]. After *C. tropicalis* cells were treated with CGA-N9, nuclear condensation became apparent. Therefore, *C. tropicalis* cell death due to CGA-N9 shares many comparable features with yeast apoptosis. The *in vitro* investigation of the interaction of DNA with CGA-N9 showed that CGA-N9 did not damage the integrity of the DNA but bound weakly to the DNA through electrostatic attraction. Electrostatic binding, as one of the three non-covalent binding modes between DNA and small molecules, is a non-selective interaction between the DNA phosphoric acid skeleton and positive molecules [24,34,50].

In summary, CGA-N9 in *C. tropicalis* cells induces dysregulation of calcium homeostasis, which results in intracellular ROS accumulation. Under oxidative stress, mitochondrial membrane permeability increases, allowing an influx of Ca^{2+} into mitochondria and an efflux of Cyt *c* from mitochondria, leading to the disruption of the mitochondrial membrane potential, which is also a sign of apoptosis. ROS accumulation further induces chromatin condensation, which represents the late apoptosis. Therefore, CGA-N9 induces apoptosis in *C. tropicalis* by attenuating mitochondrial function.

Abbreviations

AMPs, antimicrobial peptides; Ca^{2+}, calcium ion; CFU, colony-forming unit; CGA, chromogranin A; CGA-N9, a chromogranin A-derived fragment, consisting of the 47th to the 55th amino acids of the N-terminus; CGMCC, China General Microbiological Culture Collection Center; Cyt *c*, cytochrome *c*; DAPI, 4,6-diamidino-2-phenylindole; DHR123, dihydrorhodamine-123; DiSC(3)5, 3,3′-dipropylthiadicarbocyanine iodide; EB, ethidium bromide; FITC, fluorescein isothiocyanate; FL1-H, the first fluorescence channel; MIC, minimum inhibitory concentration; mPTP, mitochondrial permeability transition pore; PBS, phosphate-buffered saline; ROS, reactive oxygen species; SSC-H, side scatter channel; UV, ultraviolet.

Author Contribution

Ruifang Li drafted the manuscript and participated in the design and coordination of the experiments. Chen Chen carried out the experiments. Beibei Zhang provided guidance for the experiments. Hongjuan Jing and Zichao Wang participated in the final editing of the manuscript. Chunling Wu and Pu Hao assisted Chen Chen with the confocal microscopy experiments. Yong Kuang and Minghang Yang participated in the peptide synthesis. All authors have read and approved the final manuscript.

Funding

This study was supported by the National Natural Science Foundation of China (31572264 and 31071922), the Innovative Research Team (in Science and Technology) at the University of Henan Province (19IRTSTHN008), and the National Engineering Laboratory for Wheat & Corn Further Processing, Henan University of Technology (NL2016010).

Competing Interests

The Authors declare that there are no competing interests associated with the manuscript.

References

1 Perfect, J.R. (2017) The antifungal pipeline: a reality check. *Nat. Rev. Drug Discov.* **16**, 603–616 https://doi.org/10.1038/nrd.2017.46
2 Nur, Y. (2014) Epidemiology and risk factors for invasive candidiasis. *Ther. Clin. Risk Manag.* **10**, 95–105 https://doi.org/10.2147/TCRM.S40160
3 Guinea, J. (2014) Global trends in the distribution of *Candida* species causing candidemia. *Clin. Microbiol. Infect.* **20**, 5–10 https://doi.org/10.1111/1469-0691.12539
4 Wisplinghoff, H., Ebbers, J., Geurtz, L., Stefanik, D., Major, Y., Edmond, M.B. et al. (2014) Nosocomial bloodstream infections due to *Candida* spp. in the USA: species distribution, clinical features and antifungal susceptibilities. *Int. J. Antimicrobial Agents* **43**, 78–81 https://doi.org/10.1016/j.ijantimicag.2013.09.005
5 Kett, D.H., Azoulay, E., Echeverria, P.M. and Vincent, J.L. (2011) Candidabloodstream infections in intensive care units: analysis of the extended prevalence of infection in intensive care unit study. *Crit. Care Med.* **39**, 665–670 https://doi.org/10.1097/CCM.0b013e318206c1ca
6 Chai, L.Y.A., Denning, D.W. and Warn, P. (2010) *Candida tropicalis* in human disease. *Crit. Rev. Microbiol.* **36**, 282–298 https://doi.org/10.3109/1040841X.2010.489506
7 Pfaller, M.A. (2012) Antifungal drug resistance: mechanisms, epidemiology, and consequences for treatment. *Amer. J. Med.* **125**, 3–13 https://doi.org/10.1016/j.amjmed.2011.11.001
8 Yeaman, M.R. and Yount, N.Y. (2003) Mechanisms of antimicrobial peptide action and resistance. *Pharmacol. Rev.* **55**, 27–55 https://doi.org/10.1124/pr.55.1.2
9 Hu, K., Jiang, Y., Xie, Y., Liu, H., Liu, R., Zhao, Z. et al. (2015) Small-anion selective transmembrane “holes” induced by an antimicrobial peptide too short to span membranes. *J. Phys. Chem. B* **119**, 8553–8560 https://doi.org/10.1021/acs.jpcb.5b03133
10 Guaní-guerra, E., Santos-mendoza, T., Lugo-reyes, S.O. and Terán, L.M. (2010) Antimicrobial peptides: general overview and clinical implications in human health and disease. *Clin. Immunol.* **135**, 1–11 https://doi.org/10.1016/j.clim.2009.12.004
11 Wiesner, J. and Vilcinskas, A. (2010) Antimicrobial peptides: the ancient arm of the human immune system. *Virulence* **1**, 440–464 https://doi.org/10.4161/viru.1.5.12983
12 Helman, L.J., Ahn, T.G., Levine, M.A., Allison, A., Cohen, P.S., Cooper, M.J. et al. (1988) Molecular cloning and primary structure of human chromogranin a (secretory protein I) cDNA. *J. Biol. Chem.* **263**, 11559–11563 https://doi.org/10.1287/moor.27.3.567.317
13 Li, R., Chen, C., Zhu, S., Wang, X., Yang, Y., Shi, W. et al. (2019) CGA-N9, an antimicrobial peptide derived from chromogranin A: direct cell penetration of and endocytosis by *Candida tropicalis*. *Biochem. J.* **476**, 483–497 https://doi.org/10.1042/BCJ20180801
14 Dong, W., Mao, X., Guan, Y., Kang, Y. and Shang, D. (2017) Antimicrobial and anti-inflammatory activities of three chensinin-1 peptides containing mutation of glycine and histidine residues. *Sci. Rep.* **7**, 40228 https://doi.org/10.1038/srep40228
15 Veldhuizen, E.J.A., Schneider, V.A.F., Agustiandari, H., Van Dijk, A., Tjeerdsma-Van Bokhoven, J.L.M., Bikker, F.J. et al. (2014) Antimicrobial and immunomodulatory activities of pr-39 derived peptides. *PLoS ONE* **9**, e95939 https://doi.org/10.1371/journal.pone.0095939
16 Lee, H., Hwang, J.-S. and Lee, D.G. (2017) Scolopendin, an antimicrobial peptide from centipede, attenuates mitochondrial functions and triggers apoptosis in *Candida albicans*. *Biochem. J.* **474**, 635–645 https://doi.org/10.1042/BCJ20161039
17 Tian, J., Lu, Z., Wang, Y., Zhang, M., Wang, X., Tang, X. et al. (2017) Nerol triggers mitochondrial dysfunction and disruption via elevation of Ca^{2+}, and ROS in *Candida albicans*. *Int. J. Biochem. Cell Biol.* **85**, 114–122 https://doi.org/10.1016/j.biocel.2017.02.006
18 Park, C. and Lee, D.G. (2010) Melittin induces apoptotic features in *Candida albicans*. *Biochem. Biophys. Res. Commun.* **394**, 170–172 https://doi.org/10.1016/j.bbrc.2010.02.138

Biochemical Journal (2019) **476** 3069–3080
https://doi.org/10.1042/BCJ20190483

19 Yun, J.E., Woo, E.R. and Lee, D.G. (2016) Isoquercitrin, isolated from aster yomena triggers ROS-mediated apoptosis in *Candida albicans*. *J. Funct. Foods* **22**, 347–357 https://doi.org/10.1016/j.jff.2016.01.041
20 Li, R., Zhang, R., Yang, Y., Wang, X., Yi, Y., Fan, P. et al. (2018) CGA-N12, a peptide derived from chromogranin A, promotes apoptosis of *Candida tropicalis* by attenuating mitochondrial functions. *Biochem. J.* **475**, 1385–1396 https://doi.org/10.1042/BCJ20170894
21 Zottich, U., Da Cunha, M., Carvalho, A.O., Dias, G.B., Casarin, N., Vasconcelos, I.M. et al. (2013) An antifungal peptide from coffea canephora seeds with sequence homology to glycine-rich proteins exerts membrane permeabilization and nuclear localization in fungi. *Biochim. Biophys. Acta* **1830**, 3509–3516 https://doi.org/10.1016/j.bbagen.2013.03.007
22 Madeo, F., Fröhlich, E. and Fröhlich, K.U. (1997) A yeast mutant showing diagnostic markers of early and late apoptosis. *J. Cell Biol.* **139**, 729–734 https://doi.org/10.1083/jcb.139.3.729
23 Alfred, R.L., Palombo, E.A., Panozzo, J.F., Bhave, M. and Van Damme, E.J.M. (2013) The antimicrobial domains of wheat puroindolines are cell-penetrating peptides with possible intracellular mechanisms of action. *PLoS ONE* **8**, e75488 https://doi.org/10.1371/journal.pone.0075488
24 Rehman, S.U., Sarwar, T., Ishqi, H.M., Husain, M.A., Hasan, Z. and Tabish, M. (2015) Deciphering the interactions between chlorambucil and calf thymus DNA: a multi-spectroscopic and molecular docking study. *Arch. Biochem. Biophys.* **566**, 7–14 https://doi.org/10.1016/j.abb.2014.12.013
25 Carraro, M. and Bernardi, P. (2016) Calcium and reactive oxygen species in regulation of the mitochondrial permeability transition and of programmed cell death in yeast. *Cell Calcium* **60**, 102–107 https://doi.org/10.1016/j.ceca.2016.03.005
26 Simon, H.U., Haj-Yehia, A. and Levi-Schaffer, F. (2000) Role of reactive oxygen species (ROS) in apoptosis induction. *Apoptosis* **5**, 415–418 https://doi.org/10.1023/a:1009616228304
27 Deryabina, Y., Isakova, E., Antipov, A. and Saris, N.E.L. (2013) The inhibitors of antioxidant cell enzymes induce permeability transition in yeast mitochondria. *J. Bioenerg. Biomembr.* **45**, 491–504 https://doi.org/10.1007/s10863-013-9511-2
28 Perrone, G.G., Tan, S.X. and Dawes, I.W. (2008) Reactive oxygen species and yeast apoptosis. *Biochim. Biophys. Acta Mol. Cell Res.* **1783**, 1354–1368 https://doi.org/10.1016/j.bbamcr.2008.01.023
29 Brookes, P.S., Yoon, Y., Robotham, J.L., Anders, M.W. and Sheu, S.S. (2004) Calcium, ATP, and ROS: a mitochondrial love-hate triangle. *Am. J. Physiol. Cell Physiol.* **287**, 817–833 https://doi.org/10.1152/ajpcell.00139.2004
30 Reers, M., Smith, T.W. and Chen, L.B. (1991) J-aggregate formation of a carbocyanine as a quantitative fluorescent indicator of membrane potential. *Biochem.* **30**, 4480–4486 https://doi.org/10.1021/bi00232a015
31 Wang, C. and Youle, R.J. (2009) The role of mitochondria in apoptosis. *Annu. Rev. Genet.* **43**, 11–22 https://doi.org/10.5483/BMBRep.2008.41.1.011
32 Kapuscinski, J. (1995) DAPI: a DNA-specific fluorescent probe. *Biotech. Histochem.* **70**, 220–233 https://doi.org/10.3109/10520299509108199
33 Gupta, S.S., Ton, V.K., Beaudry, V., Rulli, S., Cunningham, K. and Rao, R. (2003) Antifungal activity of amiodarone is mediated by disruption of calcium homeostasis. *J. Biol. Chem.* **278**, 28831–28839 https://doi.org/10.1074/jbc.m303300200
34 Sarwar, T., Rehman, S.U., Husain, M.A., Ishqi, H.M. and Tabish, M. (2015) Interaction of coumarin with calf thymus DNA: deciphering the mode of binding by in vitro studies. *Int. J. Biol. Macromol.* **73**, 9–16 https://doi.org/10.1016/j.ijbiomac.2014.10.017
35 Aerts, A.M., Carmona-Gutierrez, D., Lefevre, S., Govaert, G., François, I.E.J.A., Madeo, F. et al. (2009) The antifungal plant defensin RsAFP2 from radish induces apoptosis in a metacaspase independent way in candida albicans. *FEBS Lett.* **583**, 2513–2516 https://doi.org/10.1016/j.febslet.2009.07.004
36 Morton, C.O., Santos, S.C.D. and Coote, P. (2007) An amphibian-derived, cationic, α-helical antimicrobial peptide kills yeast by caspase-independent but AIF-dependent programmed cell death. *Mol. Microbiol.* **65**, 494–507 https://doi.org/10.1111/j.1365-2958.2007.05801.x
37 Cui, J., Kaandorp, J.A., Ositelu, O.O., Beaudry, V., Knight, A., Nanfack, Y.F. et al. (2009) Simulating calcium influx and free calcium concentrations in yeast. *Cell Calcium* **45**, 123–132 https://doi.org/10.1016/j.ceca.2008.07.005
38 Herrero, E., Ros, J., Belli, G. and Cabiscol, E. (2008) Redox control and oxidative stress in yeast cells. *Biochim. Biophys. Acta* **1780**, 1217–1235 https://doi.org/10.1016/j.bbagen.2007.12.004
39 Hajnóczky, G., Csordás, G., Das, S., Garcia-Perez, C., Saotome, M., Roy, S.S. et al. (2006) Mitochondrial calcium signalling and cell death: approaches for assessing the role of mitochondrial ca^{2+} uptake in apoptosis. *Cell Calcium* **40**, 553–560 https://doi.org/10.1016/j.ceca.2006.08.016
40 Khan, A., Ahmad, A., Khan, L.A. and Manzoor, N. (2014) Ocimum sanctum (l.) essential oil and its lead molecules induce apoptosis in *Candida albicans*. *Res. Microbiol.* **165**, 411–419 https://doi.org/10.1016/j.resmic.2014.05.031
41 Choi, H., Hwang, J.-S. and Lee, D.G. (2014) Identification of a novel antimicrobial peptide, scolopendin 1, derived from centipede *Scolopendra subspinipes mutilans* and its antifungal mechanism. *Insect Mol. Biol.* **23**, 788–799 https://doi.org/10.1111/imb.12124
42 Hwang, J.H., Hwang, I.S., Liu, Q.H., Woo, E.R. and Lee, D.G. (2012) (+)-medioresinol leads to intracellular ROS accumulation and mitochondria-mediated apoptotic cell death in *Candida albicans*. *Biochimie* **94**, 1784–1793 https://doi.org/10.1016/j.biochi.2012.04.010
43 Sena, L.A. and Chandel, N.S. (2012) Physiological roles of mitochondrial reactive oxygen species. *Mol. Cell* **48**, 158–167 https://doi.org/10.1016/j.molcel.2012.09.025
44 Gottlieb, E., Armour, S.M., Harris, M.H. and Thompson, C.B. (2003) Mitochondrial membrane potential regulates matrix configuration and cytochrome c release during apoptosis. *Cell Death and Differ.* **10**, 709–717 https://doi.org/10.1038/sj.cdd.4401231
45 Krysko, D.V., Roels, F., Leybaert, L. and D'Herde, K. (2001) Mitochondrial transmembrane potential changes support the concept of mitochondrial heterogeneity during apoptosis. *J. Histochem. Cytochem.* **49**, 1277–1284 https://doi.org/10.1177/002215540104901010
46 Ludovico, P., Rodrigues, F., Almeida, A., Silva, M.T., Barrientos, A. and Côrte-Real, M. (2002) Cytochrome c release and mitochondria involvement in programmed cell death induced by acetic acid in *Saccharomyces cerevisiae*. *Mol. Biol. Cell* **13**, 2598–2606 https://doi.org/10.1091/mbc.e01-12-0161
47 Pereira, C., Camougrand, N., Manon, S., Sousa, M.J. and Côrte-Real, M. (2007) ADP/ATP carrier is required for mitochondrial outer membrane permeabilization and cytochrome c release in yeast apoptosis. *Mol. Microbiol.* **66**, 571–582 https://doi.org/10.1111/j.1365-2958.2007.05926.x
48 Sedelnikova, O.A., Redon, C.E., Dickey, J.S., Nakamura, A.J., Georgakilas, A.G. and Bonner, W.M. (2010) Role of oxidatively induced DNA lesions in human pathogenesis. *Mutat. Res.* **704**, 152–159 https://doi.org/10.1016/j.mrrev.2009.12.005
49 Ribeiro, G.F., Côrte-Real, M. and Johansson, B. (2006) Characterization of DNA damage in yeast apoptosis induced by hydrogen peroxide, acetic acid, and hyperosmotic shock. *Mol. Biol. Cell* **17**, 4584–4591 https://doi.org/10.1091/mbc.e06-05-0475
50 Bera, R., Sahoo, B.K., Ghosh, K.S. and Dasgupta, S. (2008) Studies on the interaction of isoxazolcurcumin with calf thymus DNA. *Int. J. Biol. Macromol.* **42**, 12–21 https://doi.org/10.1016/j.ijbiomac.2007.08.010

